Figure F1. Broadband radio data for G4Jy sources that also appear in the 3CRR sample (Section 7.3 and Appendix F of White et al. 2020a). Red datapoints are total, integrated flux-densities from GLEAM (Section 6.5), and blue datapoints are flux densities from Laing & Peacock (1980). Fitted to all data is a power-law function (orange, solid line) and a curved model (black, dashed line; Callingham et al., 2017) to guide the eye. Note that the curved fit is largely being dominated by small uncertainties associated with the high-frequency data, and that sudden 'up-turns' in the GLEAM flux-densities are likely due to the calibration failing for particular sub-bands.

Sarah V. White et al.

(a) G4Jy 161

(b) G4Jy 174

(c) G4Jy 179

(d) G4Jy 206
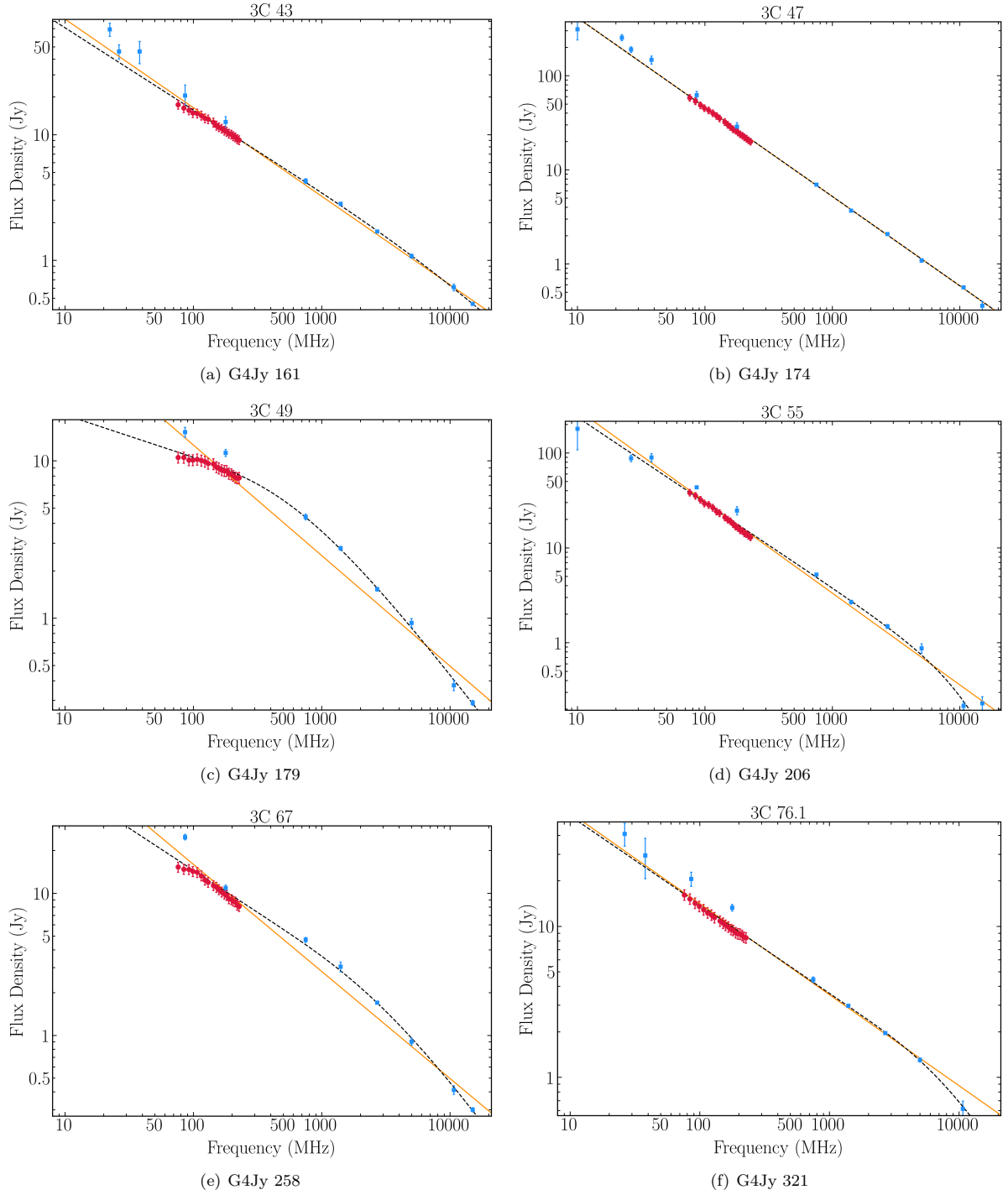
(e) G4Jy 258

(f) G4Jy 321

Figure F2. Broadband radio data for G4Jy sources that also appear in the 3CRR sample (Section 7.3 and Appendix F of White et al. 2020a). The datapoints and lines are as described for Figure F1.
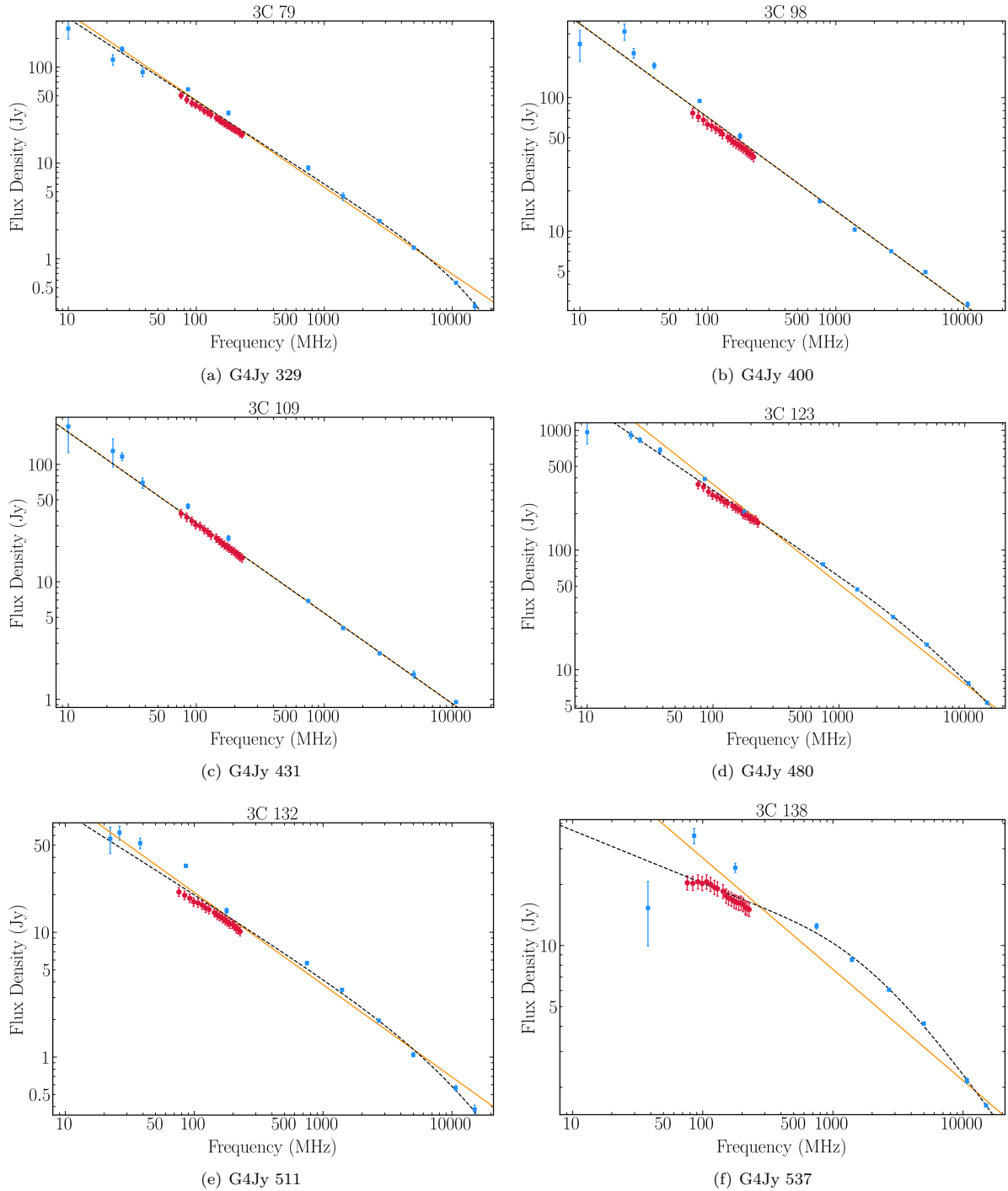
(a) G4Jy 329

(b) G4Jy 400

(c) G4Jy 431

(d) G4Jy 480

(e) G4Jy 511

(f) G4Jy 537

Figure F3. Broadband radio data for G4Jy sources that also appear in the 3CRR sample (Section 7.3 and Appendix F of White et al. 2020a). The datapoints and lines are as described for Figure F1.
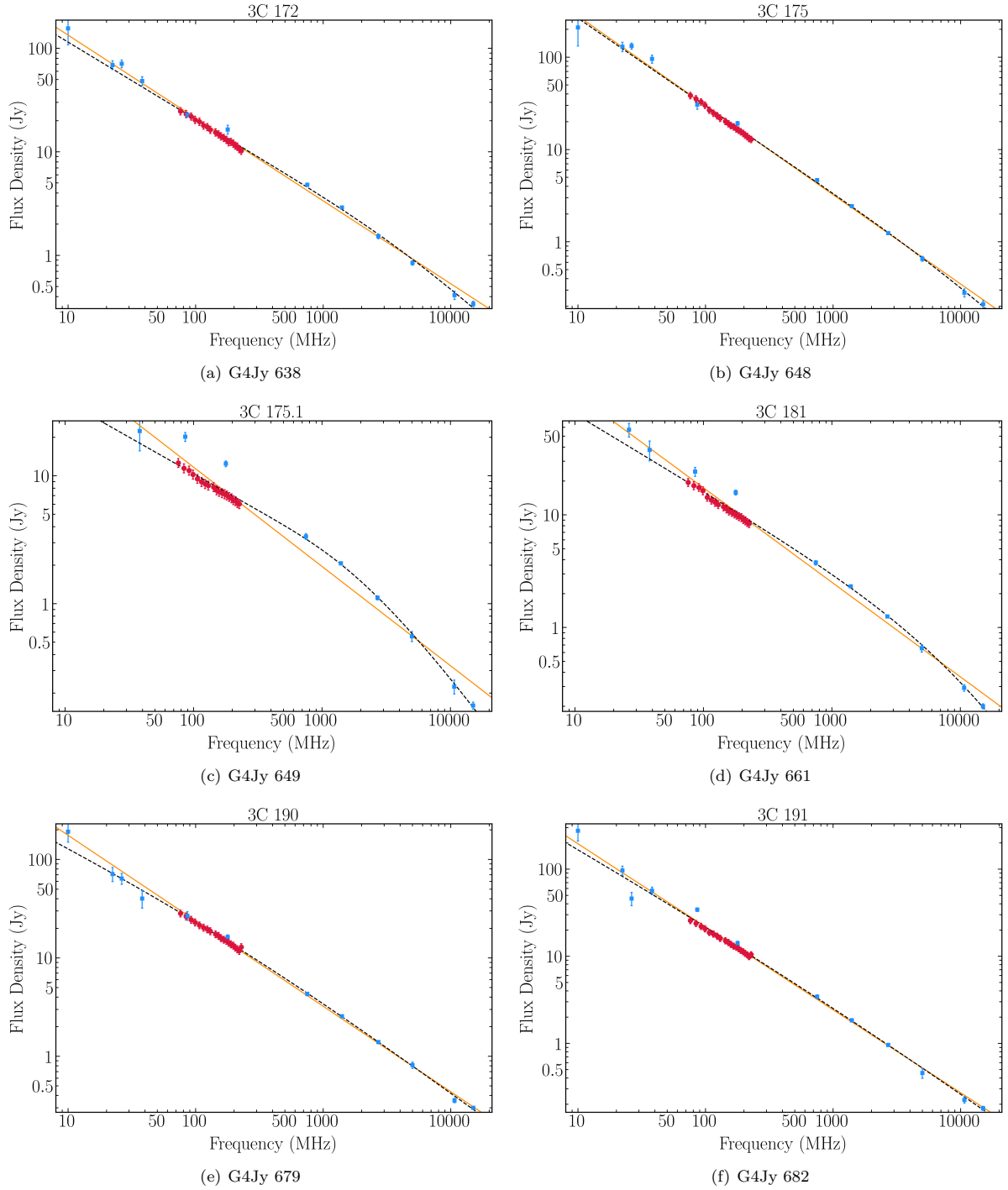
(a) G4Jy 638

(b) G4Jy 648

(c) G4Jy 649

(d) G4Jy 661

(e) G4Jy 679

(f) G4Jy 682

Figure F4. Broadband radio data for G4Jy sources that also appear in the 3CRR sample (Section 7.3 and Appendix F of White et al. 2020a). The datapoints and lines are as described for Figure F1.
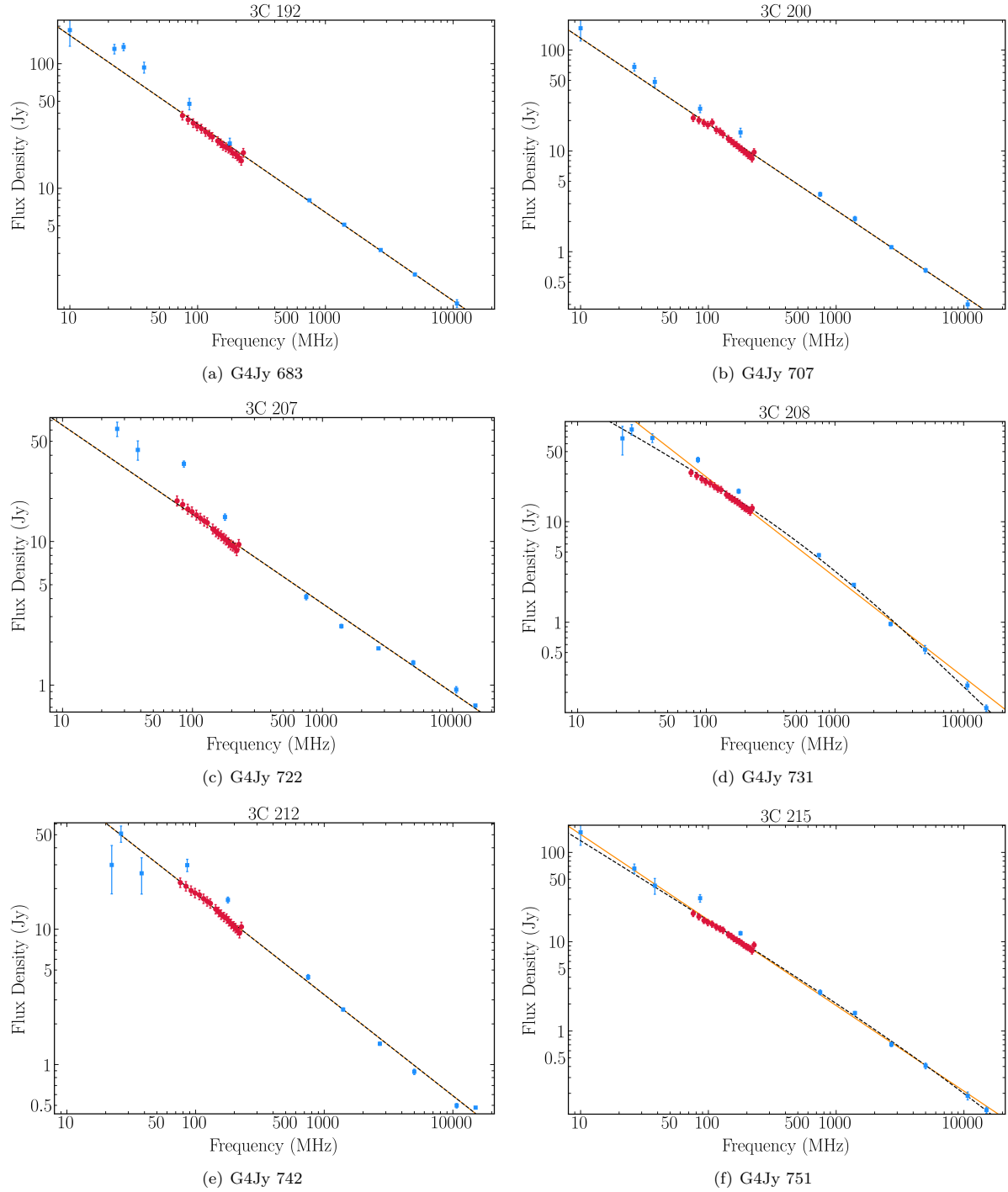
(a) G4Jy 683

(b) G4Jy 707

(c) G4Jy 722

(d) G4Jy 731

(e) G4Jy 742

(f) G4Jy 751

Figure F5. Broadband radio data for G4Jy sources that also appear in the 3CRR sample (Section 7.3 and Appendix F of White et al. 2020a). The datapoints and lines are as described for Figure F1.
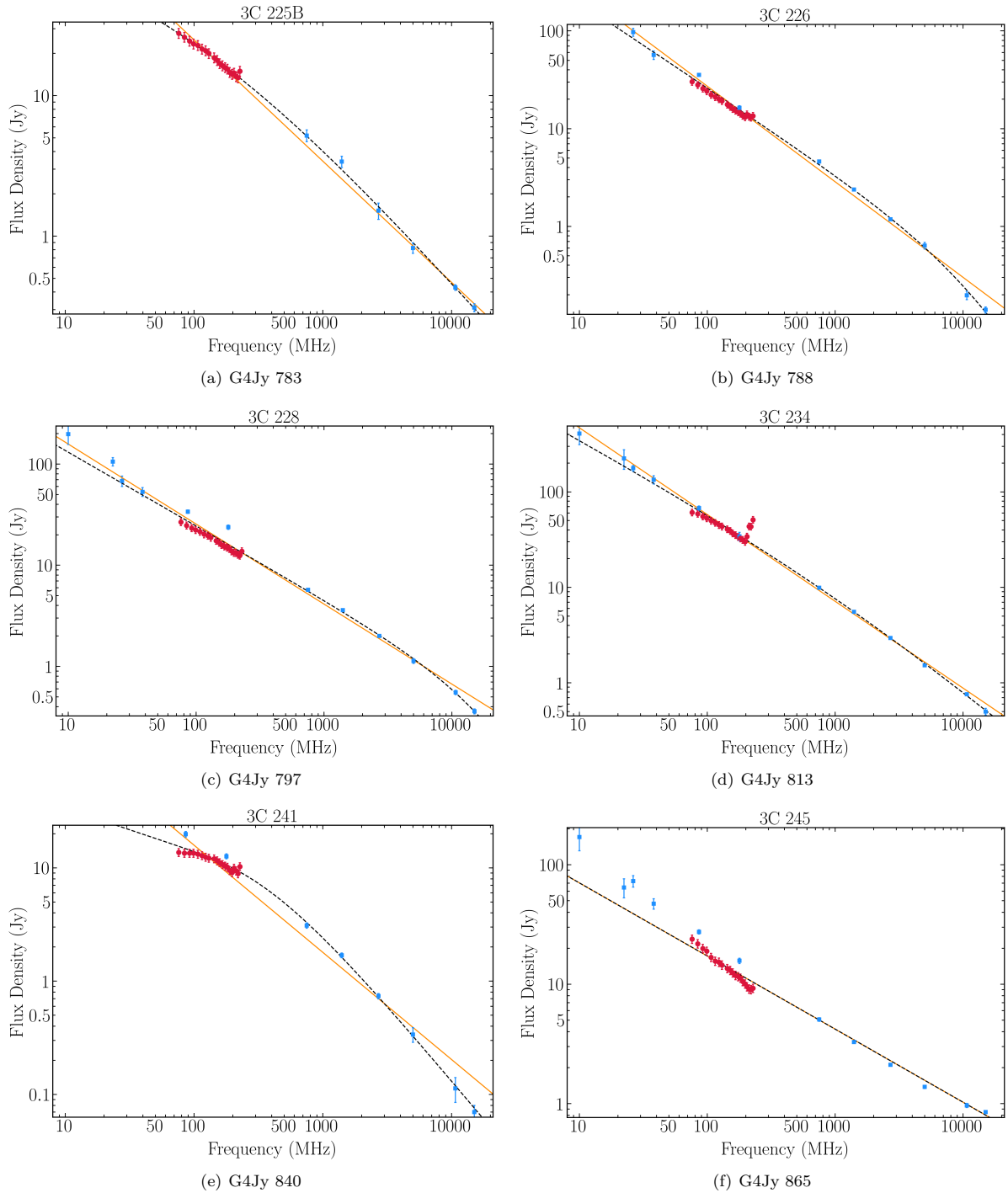
(a) G4Jy 783

(b) G4Jy 788

(c) G4Jy 797

(d) G4Jy 813

(e) G4Jy 840

(f) G4Jy 865

Figure F6. Broadband radio data for G4Jy sources that also appear in the 3CRR sample (Section 7.3 and Appendix F of White et al. 2020a). The datapoints and lines are as described for Figure F1.
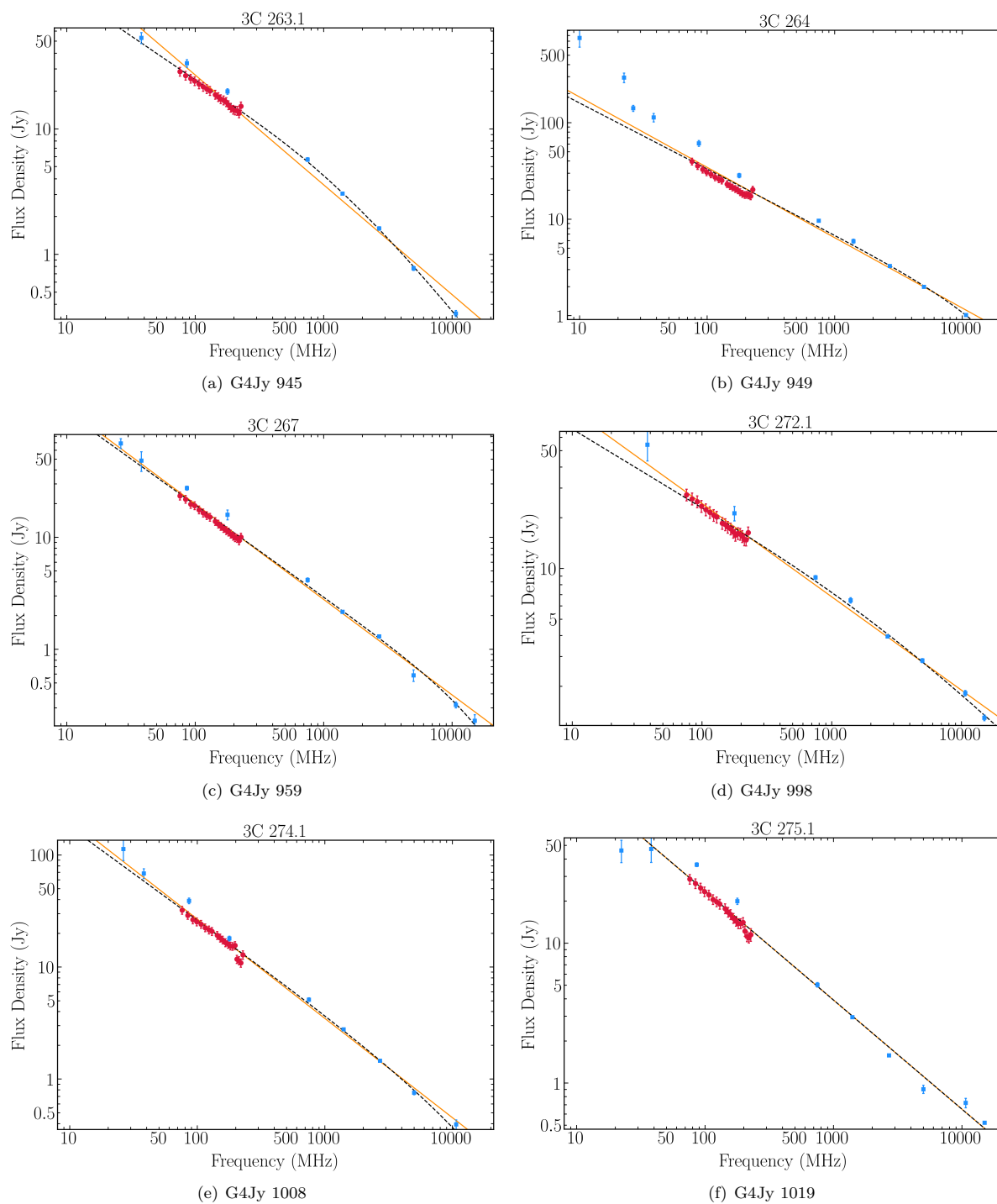
(a) G4Jy 945

(b) G4Jy 949

(c) G4Jy 959

(d) G4Jy 998

(e) G4Jy 1008

(f) G4Jy 1019

Figure F7. Broadband radio data for G4Jy sources that also appear in the 3CRR sample (Section 7.3 and Appendix F of White et al. 2020a). The datapoints and lines are as described for Figure F1.
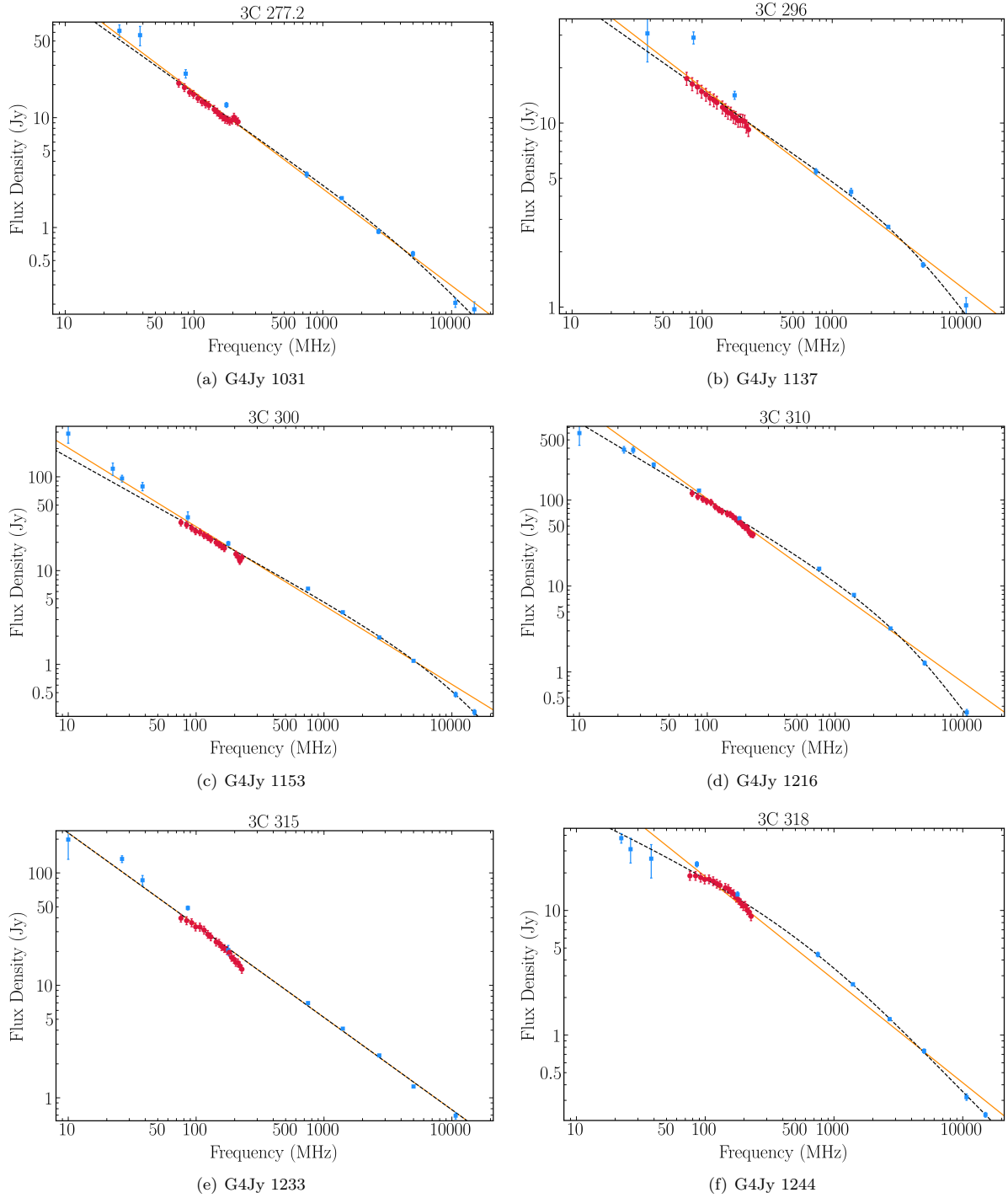
(a) G4Jy 1031

(b) G4Jy 1137

(c) G4Jy 1153

(d) G4Jy 1216

(e) G4Jy 1233

(f) G4Jy 1244

Figure F8. Broadband radio data for G4Jy sources that also appear in the 3CRR sample (Section 7.3 and Appendix F of White et al. 2020a). The datapoints and lines are as described for Figure F1.

Figure F9. Broadband radio data for G4Jy sources that also appear in the 3CRR sample (Section 7.3 and Appendix F of White et al. 2020a). The datapoints and lines are as described for Figure F1.
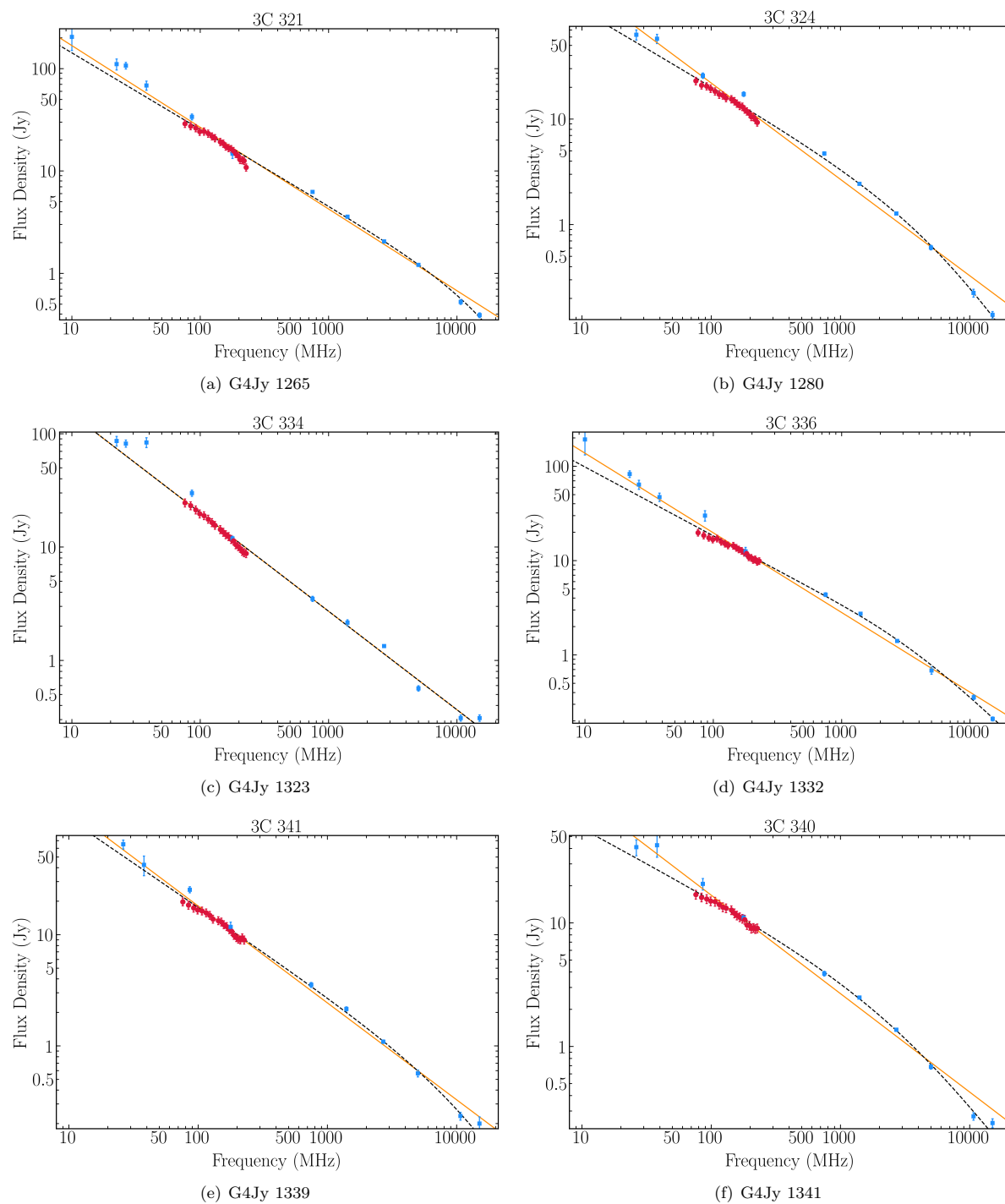
(a) G4Jy 1358

(b) G4Jy 1460

(c) G4Jy 1499

(d) G4Jy 1690

(e) G4Jy 1719

(f) G4Jy 1724

Figure F10. Broadband radio data for G4Jy sources that also appear in the 3CRR sample (Section 7.3 and Appendix F of White et al. 2020a). The datap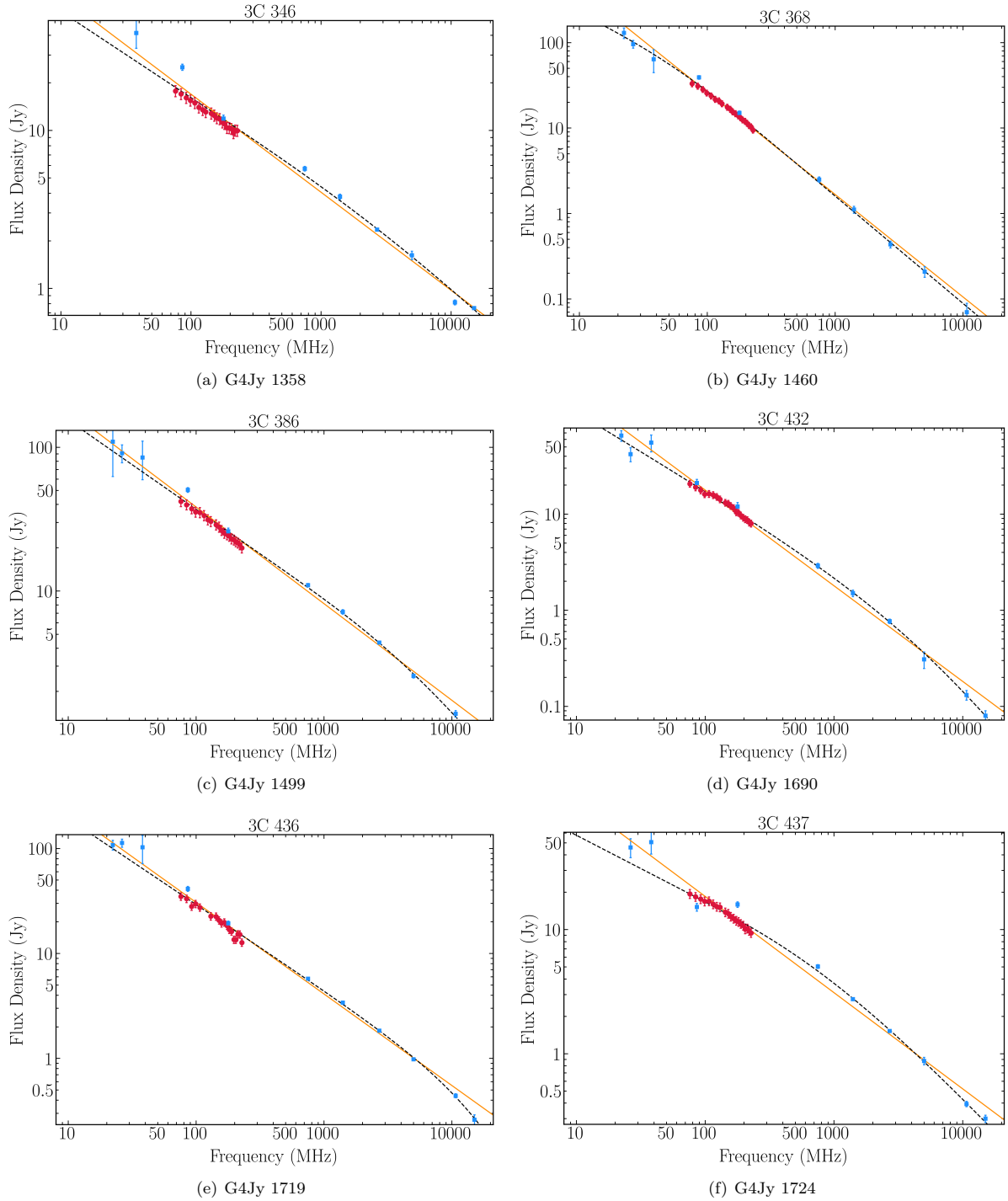oints and lines are as described for Figure F1.